PROCEEDINGS OF SCIENCE

The cosmic-ray energy spectrum above 10^{16} eV measured with the LOFAR Radboud Air Shower Array

S. Thoudam[*,1], **S. Buitink**[2], **A. Corstanje**[1], **J.E. Enriquez**[1], **H. Falcke**[1,3,4], **J.R. Hörandel**[1,3], **A. Nelles**[1,5], **J.P. Rachen**[1], **L. Rossetto**[1], **P. Schellart**[1], **O. Scholten**[6,7], **S. ter Veen**[1,4], **T.N.G. Trinh**[6], **L. van Kessel**[1]

1 *Department of Astrophysics/IMAPP, Radboud University Nijmegen, P.O. Box 9010, 6500 GL Nijmegen, The Netherlands*
2 *Astrophysical Institute, Vrije Universiteit Brussel, Pleinlaan 2, 1050 Brussels, Belgium*
3 *NIKHEF, Science Park Amsterdam, 1098 XG Amsterdam, The Netherlands*
4 *Netherlands Institute of Radio Astronomy (ASTRON), Postbus 2, 7990 AA Dwingeloo, The Netherlands*
5 *Now at: Department of Physics and Astronomy, University of California Irvine, Irvine, CA 92697-4575, USA*
6 *KVI-CART, University Groningen, P.O. Box 72, 9700 AB Groningen, The Netherlands*
7 *Interuniversity Institute for High-Energy, Vrije Universiteit Brussel, Pleinlaan 2, 1050 Brussels, Belgium*
E-mail: s.thoudam@astro.ru.nl

The LOFAR Radboud Air Shower Array (LORA) is an array of 20 plastic scintillation detectors installed in the center of the LOFAR radio telescope in the Netherlands to measure extensive air showers induced by cosmic rays in the Earth's atmosphere. The primary goals of LORA are to trigger the read-out of the LOFAR radio antennas to record radio signals from air showers, and to assist the reconstruction of air shower properties with LOFAR by providing basic air shower parameters, such as the position of the shower axis on the ground, the arrival direction and the energy of the incoming cosmic ray. In this paper, we describe the various steps involved in the energy reconstruction of air showers measured with LORA, and present the all-particle cosmic-ray energy spectrum above 10^{16} eV reconstructed for the two extreme scenarios: pure protons and iron nuclei.

The 34th International Cosmic Ray Conference,
30 July- 6 August, 2015
The Hague, The Netherlands

*Speaker.

PoS(ICRC2015)327

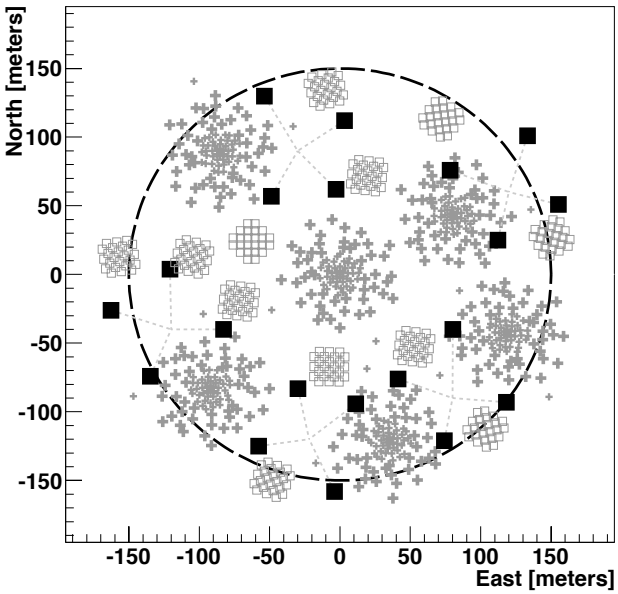

Figure 1: Schematic layout of the LORA array. *Filled squares*: LORA detectors, *crosses*: Low-band antennas, and *empty squares*: High-band antennas. The dashed circle shows a fiducial region of 150 m radius applied in our analysis.

1. Introduction

LOFAR (the Low Frequency Array), an astronomical radio telescope [1], is capable of measuring cosmic rays of energies above $\sim 10^{16}$ eV by detecting radio emission from extensive air showers in the frequency range of $10-240$ MHz [2]. The main goals of the LOFAR key science project Cosmic Rays are to measure the mass composition of cosmic rays in the energy region around $10^{16}-10^{18}$ eV [3], and to study the nature and production mechanisms of radio emission from air showers [4, 5, 6]. In order to complement this endeavour, we have set up a particle detector array, LORA (LOFAR Radboud Air Shower Array), in the core of LOFAR [7]. The primary purposes of the array are to trigger LOFAR to register radio signals from air showers, and to provide basic air shower parameters like the arrival direction, position of the shower axis on the ground, and the energy of the incoming cosmic-ray particle. In the following, we will describe the procedures we have followed for the energy reconstruction of air showers measured with LORA, and present the all-particle energy spectrum of cosmic rays above 10^{16} eV, reconstructed assuming that cosmic rays consist only of protons or iron nuclei [8].

2. LORA experiment

LORA consists of an array of 20 plastic scintillation detectors of size 0.95 m$\times$0.95 m each[1]. The detectors are distributed over a circular area having $\sim$ 300 m diameter, with spacings between

[1]The detectors were previously operated in the KASCADE calorimeter [9].

the detectors of $\sim 50-100$ m (see Figure 1). The array has been designed to measure cosmic rays of energies $\sim 10^{16}$ eV, and it is co-located with six LOFAR stations (each station consists of 96 low-band antennas and 48 high-band antennas operating in the frequency range of $10-80$ MHz and $110-240$ MHz respectively). The array is sub-divided into five units, and each unit comprises of four detectors. A local trigger configuration of 3 out of 4 detectors is set for each unit, and the full array is read-out when at least one unit is triggered. A high-level trigger is formed to read-out the LOFAR radio antennas when at least 13 out of the 20 LORA detectors are triggered. For more technical details, see Ref. [7].

3. Data analysis

The present analysis will use data collected with the LORA array during June 2011-October 2014. This amounts to a total of 707 days of data with all 20 detectors in operation, and a total of 1.8 million air showers. For each measured shower, the arrival direction of the primary cosmic ray is determined from the relative signal arrival times between the detectors. The energy deposits in each detector is used to reconstruct the position of the shower axis and the number of air shower particles at the ground (shower size). The reconstruction basically involves determining the particle density in each detector, and then performing an iterative fitting of the two-dimensional particle density distribution (projected onto the shower plane) with a lateral distribution function, the so-called NKG (Nishimura-Kamata-Greisen) function [10, 11], given by

$$\rho(r) = N_{\rm ch} C(s) \left(\frac{r}{r_{\rm M}}\right)^{s-2} \left(1+\frac{r}{r_{\rm M}}\right)^{s-4.5}, \tag{3.1}$$

where $\rho(r)$ represents the particle density in the shower plane at a radial distance r from the shower axis, $N_{\rm ch}$ is the shower size, s is shower age, $r_{\rm M}$ is the radius parameter, and the function $C(s)$ is given by,

$$C(s) = \frac{\Gamma(4.5-s)}{2\pi r_{\rm M}^2 \Gamma(s)\Gamma(4.5-2s)}. \tag{3.2}$$

Details about the fitting procedure are described in Ref. [7]. The various trigger and quality cuts applied in the analysis are listed in Table 1. Figure 2 shows the reconstructed shower size distribution for all the measured showers that survived the various cuts applied in the analysis. The peak of the distribution represents the shower size threshold of the LORA array. A Gaussian fit around the peak gives a value of $\log_{10} N_{\rm ch} = 5.92$. The distribution for four separate zenith angle bins are also shown.

4. Simulations

Simulations are performed to determine the various characteristics of the array such as the trigger and reconstruction efficiencies, the relation between the reconstructed shower size and the primary energy, and the reconstruction accuracies of shower parameters. Air showers are simulated using CORSIKA package (version 7.4387) [12] for protons and iron nuclei in the energy range of $10^{16} - 10^{19}$ eV, taking a differential energy spectrum of index -2. The showers are then weighted to generate a distribution of index -3. The zenith angle range considered is $0^\circ - 45^\circ$.

Table 1: Trigger and quality cuts applied in our analysis.

Trigger cuts:	
Single unit trigger:	3/4 detectors
Analysis:	5 detectors with ≥ 1 particle m^{-2}
Number of analysed showers:	1,861,045
Quality cuts:	
Zenith angle:	$\theta < 35^{\circ}$
Position of the shower axis:	< 150 m from array center
Radius parameter:	10 m $< r_{\rm M} <$ 200 m
Number of quality showers:	322,664

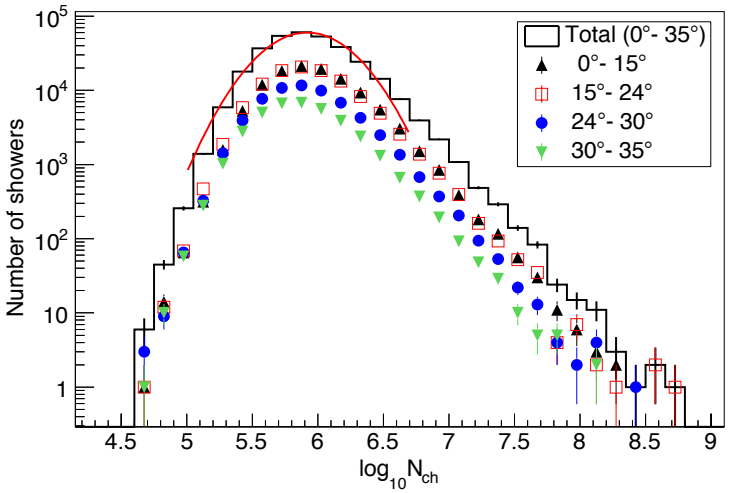

Figure 2: Reconstructed shower size distribution for the measured air showers. The line represents a Gaussian fit to the total distribution around the peak.

The energy deposition of air shower particles in the detector is simulated using GEANT4 [13] by taking into account all the important properties of the detector. The most probable energy deposition for vertical incident muons is found to be 5.3 MeV, while an all-sky muon distribution gives 6.67 MeV. The latter corresponds to an energy deposition of 400 ± 3.5 ADC counts for single particles measured with the experiment.

To improve the statistics, each simulated shower is processed 100 times with the true position of the shower axis scattered randomly within a circle of radius 160 m from the centre of the array. The reconstruction of air shower parameters for each simulated shower is performed similar to the reconstruction procedure applied to the measured data described in Section 3. The same trigger and quality cuts applied to the measurements are also applied to the simulated data. Figure 3 shows the combined trigger and reconstruction efficiencies obtained from the simulations for protons and iron nuclei as a function of the true energy $E_{\rm T}$ for four separate zenith angle bins. The full efficiency is reached at $\log_{10}(E_{\rm T}/{\rm GeV}) \approx 7.6$ for protons and at ≈ 7.7 for iron nuclei. The total acceptance of the array for the solid angle subtended within $0^{\circ} - 35^{\circ}$ is shown in Figure 4 as a function of $E_{\rm T}$.

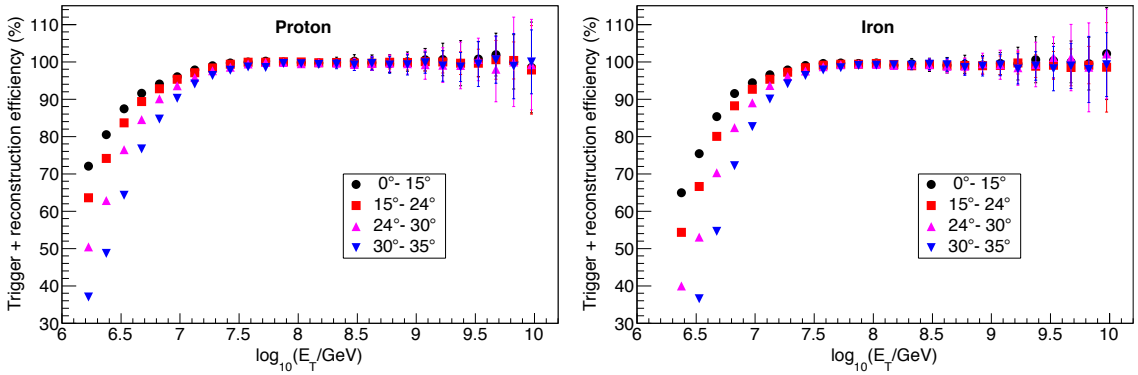

Figure 3: Combined trigger and reconstruction efficiencies for four zenith angle bins as a function of the true energy for protons (*left panel*) and iron nuclei (*right panel*).

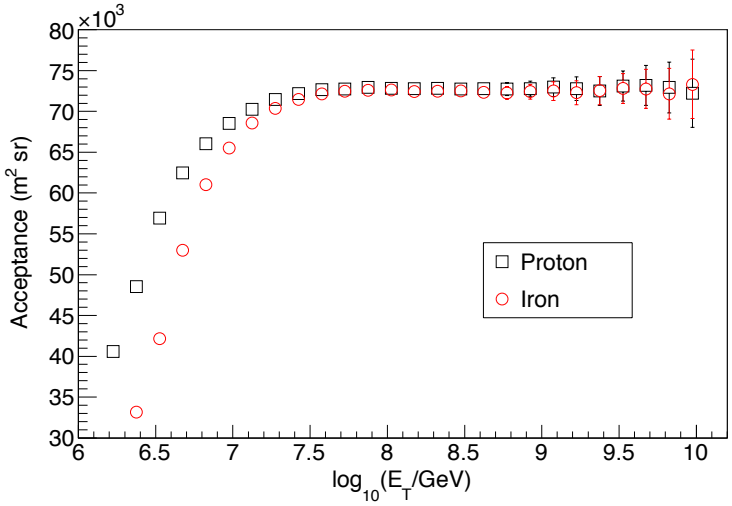

Figure 4: Total acceptance of the LORA array for solid angles subtended within $0^\circ - 35^\circ$ for protons (*squares*) and iron nuclei (*circles*).

A parameterised relation between the measured shower size and the energy of the primary particle is determined from the simulations. For this, simulated showers are binned in a two dimensional log-log histogram in the reconstructed size and the true energy. For each $\log_{10} N_{\rm ch}$ bin, the peak and the spread of the true energy distribution are obtained. The results obtained are shown in Figure 5 for different angle bins for protons and iron nuclei. The lines represent fits using the function,

$$\log_{10} E_{\rm T} = a + b \log_{10} N_{\rm ch} \tag{4.1}$$

The parameters obtained from the fits are listed in Table 2. Using those parameters, for any given simulated or measured shower for which the arrival direction and shower size have been reconstructed, the primary cosmic-ray energy can be reconstructed using the following relation,

$$\log_{10} E_{\rm R} = a + b \log_{10} N_{\rm ch}. \tag{4.2}$$

The accuracy in the energy reconstruction (energy resolution) is found to be in the range of

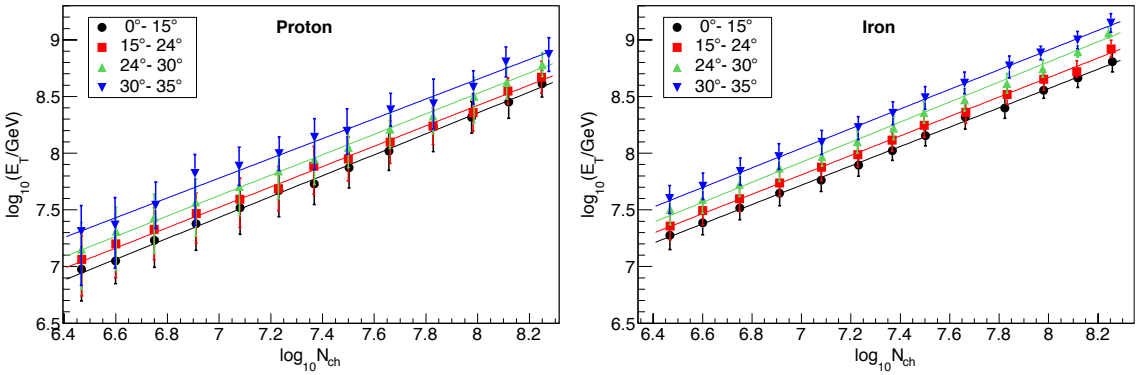

Figure 5: Relation between reconstructed size ($N_{\rm ch}$) and true energy ($E_{\rm T}$) for proton (*left panel*) and iron (*right panel*) showers for four zenith angle bins.

Table 2: Fit parameters for protons and iron nuclei obtained by fitting Equation 4.1 to the $\log_{10} N_{\rm ch} - \log_{10} E_{\rm T}$ plots shown in Figure 5 for four zenith angle bins.

Zenith angle	Protons		Iron nuclei	
θ	a	b	a	b
$0^\circ - 15^\circ$	0.980 ± 0.683	0.922 ± 0.089	1.747 ± 0.361	0.853 ± 0.048
$15^\circ - 24^\circ$	1.234 ± 0.766	0.898 ± 0.099	1.801 ± 0.370	0.858 ± 0.049
$24^\circ - 30^\circ$	1.315 ± 0.815	0.901 ± 0.101	1.726 ± 0.319	0.885 ± 0.041
$30^\circ - 35^\circ$	1.667 ± 0.692	0.873 ± 0.091	1.982 ± 0.366	0.866 ± 0.048

$\sim 28\% - 48\%$ for protons, and $\sim 12\% - 32\%$ for iron nuclei depending on the primary energy. The total systematic uncertainty in the reconstructed energy which results from the uncertainties in the energy calibration, spectral slope of the primary cosmic rays used in the simulation, energy deposition of single particle in the detector, and the hadronic interaction models used in the air shower simulation, amount to within $\sim (+20\%, -10\%)$ for protons, and within $\sim (+10\%, -5\%)$ for iron nuclei. The corresponding systematic uncertainty in the reconstructed cosmic-ray intensity is found to be $\sim (+60\%, -25\%)$ for protons, and $\sim (+38\%, -20\%)$ for iron nuclei.

5. Measured all-particle spectrum

Applying the parameterisation given by Equation 4.2, reconstructed energies are obtained on shower-by-shower basis for the measured showers that have passed through the selection cuts. The differential cosmic-ray spectrum is obtained after folding in the total acceptance of the array and the total observation time. Only the energy region for which the combined trigger and reconstruction efficiency is close to 100% is considered. Figure 6 (top panel) shows our reconstructed spectrum, assuming that cosmic rays are only protons or iron nuclei. The measured spectrum is in the range of $(1.9 \times 10^7 - 1.2 \times 10^9)$ GeV for protons, and $(2.7 \times 10^7 - 1.7 \times 10^9)$ GeV for iron nuclei. The spectra cannot be described by single power laws over the full energy range. Fitting a power spectrum below 5×10^8 GeV gives spectral slopes of $\gamma_{\rm P} = -3.18 \pm 0.13$ for protons and $\gamma_{\rm Fe} = -3.22 \pm 0.08$ for iron nuclei. In Figure 6 (bottom panel), our reconstructed spectra are compared

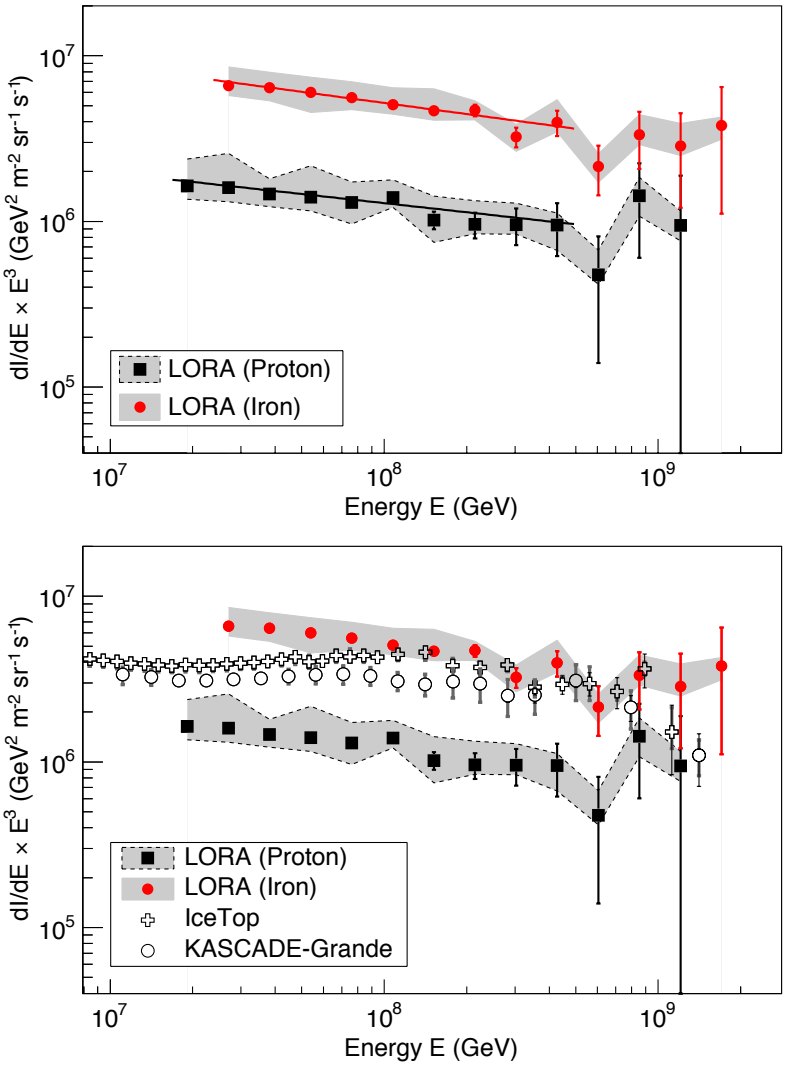

Figure 6: *Top*: All-particle cosmic-ray spectrum measured with LORA for pure protons (*squares*) and pure iron nuclei composition (*filled circles*). The error bars represent statistical uncertainties, and the shaded areas represent systematic uncertainties. The lines represent single power law fits to the measurements below 5×10^8 GeV. *Bottom*: Comparison of the LORA measurements with the results from IceTop (*crosses*) and KASCADE-Grande (*empty circles*) experiments.

with the measurements from IceTop [14] and KASCADE-Grande [15] experiments. Their spectra lie between our reconstructed spectra which is consistent with that expected for a mixed cosmic-ray composition. At higher energy, both their spectra are closer to our iron spectrum, while at lower energies, they lie closer to our proton spectrum. This indicates a change in the composition of cosmic rays in this energy region.

6. Conclusion

A detailed Monte-Carlo simulation has been carried out for the energy reconstruction of air

showers measured with the LORA detector array. The energy resolution of the LORA array falls within $\sim 28\% - 48\%$ for protons and $\sim 12\% - 32\%$ for iron nuclei, and the systematic uncertainty in the reconstructed energy is found to be $\sim (+20\%, -10\%)$ and $(+10\%, -5\%)$ for protons and iron nuclei respectively. By applying the reconstruction method to the measured air shower data, the all-particle cosmic-ray spectrum has been reconstructed for energies above 10^{16} eV for a pure proton and pure iron composition. In the future, we will combine the cosmic-ray energy measurements from LORA with the composition measurement from LOFAR in order to obtain an all-particle spectrum that takes into account the actual composition of cosmic rays.

7. Acknowledgements

The LOFAR cosmic ray key science project acknowledges funding from an Advanced Grant of the European Research Council (FP/2007-2013) / ERC Grant Agreement n. 227610. The project has also received funding from the European Research Council (ERC) under the European Union's Horizon 2020 research and innovation programme (grant agreement No 640130). We furthermore acknowledge financial support from FOM, (FOM-project 12PR304) and NWO (VENI grant 639-041-130). AN is supported by the DFG (research fellowship NE 2031/1-1).

LOFAR, the Low Frequency Array designed and constructed by ASTRON, has facilities in several countries, that are owned by various parties (each with their own funding sources), and that are collectively operated by the International LOFAR Telescope foundation under a joint scientific policy.

References

[1] van Haarlem, M., 2013, Astronomy & Astrophysics, 556, A2

[2] Schellart, P. et al., 2013, Astronomy & Astrophysics, 560, A98

[3] Buitink, S. et al., 2014, Physical Review D, 90, 082003

[4] Schellart, P. et al., 2014, Journal of Cosmology and Astroparticle Physics, 10, 014

[5] Corstanje, A. et al., 2015, Astroparticle Physics, 61, 22

[6] Nelles, A. et al., 2015, Astroparticle Physics, 65, 11

[7] Thoudam, S. et al., 2014, Nuclear Instruments and Methods in Physics Research Section A, 767, 339

[8] Thoudam, S. et al., Astroparticle Physics, Accepted; arXiv:1506.09134

[9] Antoni, T., et al., 2003, Nuclear Instruments and Methods in Physics Research Section A, 513, 490

[10] Kamata, K., & Nishimura, J., 1958, Progress of Theoretical Physics, 6, 93

[11] Greisen, K., 1960, Annual Review of Nuclear and Particle Science, 10, 63

[12] Heck, D., 1998, Report FZKA, 6019

[13] Agostinelli, S. et al., 2003, Nuclear Instruments and Methods in Physics Research Section A, 506, 250

[14] Aartsen, M. G. et al, 2013, Physical Review D, 88, 042004

[15] Apel, W. D. et al., 2012, Astroparticle Physics, 36, 183